

Electron Paramagnetic Resonance Studies of Functionally Active, Nitroxide Spin-Labeled Peptide Analogues of the C-Terminus of a G-Protein α Subunit[†]

Ned Van Eps,^{||, @} Lori L. Anderson,^{‡, §, @} Oleg G. Kisselev,[⊥] Thomas J. Baranski,[§]
Wayne L. Hubbell,^{*, ||} and Garland R. Marshall^{*, ‡}

[‡]*Department of Biochemistry and Molecular Biophysics, and* [§]*Departments of Medicine, Molecular Biology and Pharmacology, Washington University, St. Louis, Missouri 63110,* ^{||}*Jules Stein Eye Institute and Department of Chemistry and Biochemistry, University of California, Los Angeles, California 90095-7008, and* [⊥]*Department of Ophthalmology and Department of Biochemistry and Molecular Biology, St. Louis University School of Medicine, St. Louis, Missouri 63104.* [@]*These authors contributed equally to this work.*

Received May 26, 2010; Revised Manuscript Received July 12, 2010

ABSTRACT: The C-terminal tail of the transducin α subunit, Gt α (340–350), is known to bind and stabilize the active conformation of rhodopsin upon photoactivation (R*). Five spin-labeled analogues of Gt α (340–350) demonstrated native-like activity in their ability to bind and stabilize R*. The spin-label 2,2,6,6-tetramethylpiperidine-1-oxyl-4-amino-4-carboxylic acid (TOAC) was employed at interior sites within the peptide, whereas a Proxyl (3-carboxyl-2,2,5,5-tetramethyl-pyrrolidinyloxy) spin-label was employed at the amino terminus of the peptide. Upon binding to R*, the electron paramagnetic resonance spectrum of TOAC³⁴³-Gt α (340–350) revealed greater immobilization of the nitroxide when compared to that of the N-terminally modified Proxyl-Gt α (340–350) analogue. A doubly labeled Proxyl/TOAC³⁴⁸-Gt α (340–350) was examined by DEER spectroscopy to determine the distribution of distances between the two nitroxides in the peptides when in solution and when bound to R*. TOAC and Proxyl spin-labels in this GPCR–G-protein α -peptide system provide unique biophysical probes that can be used to explore the structure and conformational changes at the rhodopsin–G-protein interface.

Spin-labeled proteins and peptides, as used in EPR¹ studies, provide a dynamic view of biological phenomena. In site-directed spin labeling (SDSL), nitroxide amino acids are selectively introduced into a peptide or protein, and the electron paramagnetic resonance is analyzed to provide information about sequence-specific secondary and tertiary structure, membrane protein topography, and electrostatic potential (1), conformational changes (2), protein dynamics (3), and inter-nitroxide distances (4–7). In most studies, the nitroxide side chain designated R1 has been employed (Figure 1A). Crystallographic (8–11), mutagenic (12, 13), and spectral simulation studies (14) revealed that internal motions of the side chain are constrained due to interactions of the disulfide with main chain atoms. Thus, the dynamics, and hence the EPR spectra, are primarily determined by limited torsional oscillations about two dihedral angles (angles X_4 and X_5 in Figure 1A). As a result of this constrained motion, the EPR spectrum is highly

sensitive to additional backbone fluctuations and to modulations of the motion due to interactions of the nitroxide with the local environment in the protein. Thus, the EPR spectrum is a “fingerprint” of the local structure and dynamics. For this reason, EPR spectral line shape analysis of R1 in proteins has been able to reveal and characterize conformational changes (2), in some cases with real-time resolution (15, 16). Of particular interest for this report are SDSL studies of receptor systems, including the GPCR rhodopsin (17, 18), its cognate G-protein transducin (19–23), and estrogen receptor α (24). In addition to investigation of conformational changes, EPR spectra of R1 have been analyzed to determine the amplitudes of backbone fluctuations on the nanosecond time scale (3). This is of interest because sequences with flexibility on this time scale often turn out to be involved in protein–protein recognition.

One of the most powerful tools for static structure determination in SDSL is interspin distance measurement in systems containing two nitroxide side chains. At normal physiological temperatures, interspin distances in the range of 10–20 Å can readily be measured using continuous wave (CW) EPR deconvolution methods to extract dipolar broadening (4, 5). At low temperatures, the time domain method DEER (double electron–electron resonance) extends the distance range to near 80 Å (6, 7). Most importantly, DEER resolves multiple discrete distances and their corresponding distributions, with the only disadvantage that time-resolved changes in distances are not readily monitored due to the requirement of low temperature. Thus, the range of distances between 10 and 80 Å is accessible, ideal for mapping structure and structural changes in proteins and complexes.

[†]This research was supported in part by grants from the Lucille P. Markey Predoctoral Fellowship (to L.L.A.), Chemistry Biology Interface Pathway Grant T32GM0878 (to L.L.A.), National Institutes of Health Grants GM68460, GM53630, and EY1211301 (to G.R.M.), GM71634 and GM63720 (to T.J.B.), GM63203, EY18107, and RPB (to O.G.K.), and EY05216 (to W.L.H.), and the Jules Stein Professorship endowment.

^{*}To whom correspondence should be addressed. G.R.M.: phone, (314) 362-1567; e-mail, garlandm@gmail.com. W.L.H.: phone, (310) 206-8830; fax, (310) 794-2144; e-mail, hubbellw@jsei.ucla.edu.

¹Abbreviations: EPR, electron paramagnetic resonance; TOAC, 2,2,6,6-tetramethylpiperidine-1-oxyl-4-amino-4-carboxylic acid; Proxyl, 3-carboxyl-2,2,5,5-tetramethyl-pyrrolidinyloxy, free radical; G-protein, heterotrimeric guanine nucleotide binding protein; GPCR, G-protein-coupled receptor; DEER, double electron–electron resonance.

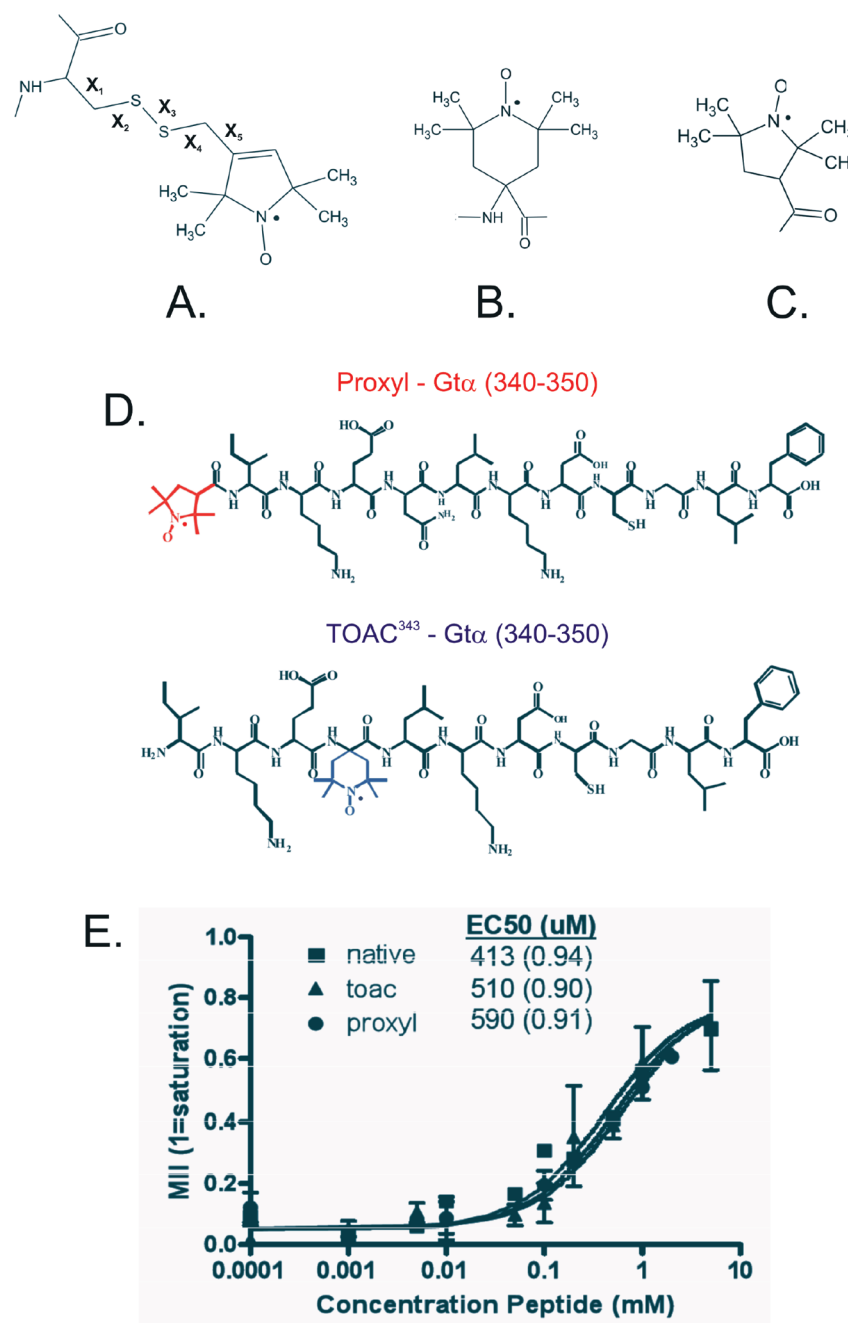


FIGURE 1: Chemical structures of spin-labels and peptides and binding of peptides to activated rhodopsin. (A) Spin-label R1 [cysteine S-(2,2,5,5-tetramethyl-2,5-dihydro-1H-pyrrol-3-yl)methyl-disulfide] used in SDSL with potential degrees of freedom indicated (X_1 – X_5 dihedrals). (B) TOAC (2,2,6,6-tetramethylpiperidine-1-oxyl-4-amino-4-carboxyl) spin-label. (C) Proxyl (2,2,5,5-tetramethyl-3-carboxyl-pyrrolidine-1-oxyl) spin-label used to modify the amino terminus. (D) Chemical structures of two spin-labeled peptides. (E) MII stabilization assay for native Gt α (340–350) compared with Proxyl-Gt α (340–350) and TOAC³⁴³-Gt α (340–350).

Although the R1 side chain has proven to be extremely useful as a monitor of local protein structure and dynamics, the inherent potential for the R1 side chain to adopt multiple rotamers in proteins warrants particular care for interpretation of interspin distances in terms of protein structure. Despite the fact that R1 has a limited conformational space at solvent-exposed sites (8–11), interactions with the protein can result in the population of higher-energy rotamers. This can be mitigated for measuring structural changes by judicious selection of sites for R1 introduction (18), but uncertainty remains for relating internitroxide distances to distances between C α atoms. This uncertainty can be overcome to some extent with sufficient distance constraints to localize the spatial position of the nitroxide, but practical applications require multiple nitroxide pairs (18).

This report explores the utility of a more constrained side chain, TOAC (Figure 1B). The tetra-substituted α,α -dialkyl spin-label TOAC (2,2,6,6-tetramethylpiperidine-1-oxyl-4-amino-4-carboxylic acid) (25) contains a nitroxide ring attached to the peptide backbone through its α -carbon (Figure 1B). Because of the self-imposed cyclic constraints of TOAC, it provides a useful tool for measuring conformational changes using DEER, since distances between TOACs are not compromised by uncertainties in rotamer distribution, but TOAC does have twist-boat ring conformers in which the 2p orbital of the nitroxide is inclined at different angles with respect to an α -helix axis (26, 27). The fixed spatial orientations of TOACs can complicate simple distance measurements, but this feature is of potential use in measuring relative orientations of structural elements in a protein (28).

The introduction of TOAC into peptide chemistry allowed the first use of linking a rigid spin-label to a growing peptide chain through an amide bond. Although incorporation of TOAC has become common in chemical synthesis because of its high sensitivity for monitoring conformational changes within the peptide scaffold, its use in biologically relevant systems is limited, as it cannot be incorporated biosynthetically and is more difficult to synthetically incorporate in peptide sequences for chemical ligation because of its lower reactivity due to steric hindrance.

Acetyl-TOAC- α -MSH (29) and N-terminal TOAC derivatives of angiotensin (30, 31) and bradykinin (31) demonstrated the first syntheses of spin-labeled peptide hormones that maintained biological activity. Furthermore, a series of three, TOAC-labeled, neuropeptide Y analogues maintained their ability to bind the G-protein-coupled receptor Y, demonstrating the ability to obtain structural information upon binding of the NPY ligand to its receptor (32). Smythe et al. (33, 34) were the first to incorporate two TOAC residues into model helical peptides for comparison with EPR studies on the more flexible SDSL label R1.

Herein, TOAC-labeled G α -transducin (G α)-terminal peptides are used to probe changes in peptide mobility that accompany binding at the GPCR rhodopsin–G-protein interface. Rhodopsin, the primary visual receptor and the prototype of G-protein-coupled receptors, is one of the best characterized of all GPCRs. Upon photoactivation, rhodopsin forms an active signaling conformation, metarhodopsin II (MII), resulting in interaction with transducin (G $\alpha\beta\gamma$), its heterotrimeric G-protein partner. Interaction between G $\alpha\beta\gamma$ and MII stabilizes the MII state and initiates a signal cascade ultimately leading to nucleotide exchange on G α resulting in dissociation of G $\alpha\beta\gamma$ from the GPCR as G $\beta\gamma$ and G α -GTP (35, 36). A synthetic undecapeptide corresponding to G α (340–350) (IKENLKDCGLF) binds to activated rhodopsin and stabilizes the MII state, thus mimicking the effects of transducin itself (37). The structure of the G α peptide bound to photoactivated rhodopsin was determined using transferred nuclear Overhauser effect (TrNOE) NMR spectroscopy (38, 39).

Results reported by Kisselev et al. demonstrated that upon light activation, G α (340–350) shifts from a highly disordered conformation to an ordered continuous helix terminated by a C-terminal capping motif, associated with the formation of a unique clustering of residues, namely, L344, K345, L349, and F350 (39). Similar structural results were obtained by Koenig et al. using transferred NOE on an analogue of G α (340–350) bound to MII (40) as well as by the crystal structure of the undecapeptide bound to opsin (41). The conformational changes that occur in the C-terminal sequence upon receptor interaction were further investigated by fluorescence and spin labeling of substituted cysteines in the G α subunit (42, 43). Further understanding these conformational changes should provide better insight into possible mechanisms of nucleotide exchange of α -subunits of G-proteins.

Here, the syntheses of spin-labeled G α peptide analogues, TOAC³⁴³-G α (340–350) and Proxyl-G α (340–350) and the doubly labeled Proxyl/TOAC³⁴⁸-G α (340–350), are reported. Each retained the ability to stabilize the MII state of rhodopsin. In addition, the analogous [TOAC³⁴³] and Proxyl analogues of the 100-fold higher-affinity peptide (VLEDLKSCGLF) reported from phage display (44) were prepared. Finally, the light-dependent binding of these analogues to native rhodopsin in disk membranes was demonstrated.

MATERIALS AND METHODS

Peptide Synthesis. Native G α (340–350) IKENLKDCGLF was synthesized on a 0.2 mmol scale via the manual Fmoc protection strategy using Fmoc-Phe-Wang resin and the following Fmoc amino acid derivatives: Fmoc-Lys(Boc), Fmoc-Glu(tBu), Fmoc-Asn(Trt), Fmoc-Asp(tBu), and Fmoc-Cys(Trt). Couplings were facilitated by 2-(1*H*-benzotriazol-1-yl)-1,1,3,3-tetramethyluronium hexafluorophosphate (HBTU) in the presence of DIPEA in DMF, with a 3-fold excess over the amino component. The crude peptide was released from the Wang resin using Reagent K (82.5% trifluoroacetic acid, 5% water, 5% thioanisole, 5% phenol, and 2.5% 1,2-ethanedithiol). After reaction for 1 h, the mixture was filtered, washed with TFA, and evaporated, and the crude peptide was precipitated with diethyl ether. The peptide was purified by preparative HPLC using a C-18 column with a 10 to 90% gradient (solvent A, 0.5% TFA in H₂O; solvent B, 0.038% TFA/90% acetonitrile/10% H₂O mixture) over 25 min. Characterization by MALDI mass spectroscopy gave the expected molecular weight (*m/z*) of 1279.53.

The synthesis of TOAC³⁴³-G α (340–350) IKE-TOAC-LKD-CGLF and the respective high-affinity analogue VLE-TOAC-LKSVGLF followed the same path described above with the following modifications. The stable nitroxide Fmoc amino acid TOAC was synthesized according to a reported procedure (45). The coupling steps involving the carboxyl and amino groups of TOAC were achieved with 5 equiv of Fmoc amino acid activated by 5 equiv of TFFH and 10 equiv of DIPEA and repeated twice for 2 h. After incorporation of TOAC and Asp, unreacted amino groups were acetylated with acetic anhydride and DMF using a catalytic amount of DMAP for 30 min. The peptide was cleaved from the resin using HF in the presence of 5% anisole. Following cleavage, the peptide was precipitated with ether, filtered, and extracted with 30% acetic acid and water. The crude peptide was submitted to alkaline treatment [0.02 M ammonium acetate (pH 9) for 3 h] to recover the paramagnetic moiety. The peptide was purified by preparative HPLC using a linear gradient from 10 to 90% B over 26 min with solvent A being 0.05 M ammonium acetate (pH 5) and solvent B being 90% acetonitrile. Characterization by electrospray ionization mass spectroscopy gave the expected molecular weights of 1363 and 1302 for the low- and high-affinity analogues, respectively.

Proxyl-G α (340–350), its respective high-affinity analogue, and the doubly labeled Proxyl/TOAC³⁴⁸-G α (340–350) were synthesized through coupling of 3-carboxy-Proxyl [3-carboxyl-2,2,5,5-tetramethyl-pyrrolidinyloxy (Aldrich, St. Louis, MO)] to the amino terminus of the peptide sequences as synthesized above. Activation of the carboxyl group of Proxyl (5 equiv) was achieved with 5 equiv of TFFH and 10 equiv of DIEA and followed by coupling twice for 2 h. Cleavage and purification were the same as those for TOAC³⁴³-G α (340–350). Analysis by electrospray ionization gave the expected molecular weights of 1448 and 1388 for the low- and high-affinity analogues, respectively, and 1531 for the doubly labeled peptide.

Preparation of Rod Outer Segments. Urea-washed rod outer segments (ROS) were prepared from dark-adapted retinas (W. L. Lawson Co., Lincoln, NE) using a sucrose gradient procedure as previously described (45). All purification steps were conducted in dim red light (Kodak safelight filter, 650 nm cutoff) at 4 °C. The final ROS samples were resuspended in a 20 mM MES buffer (pH 6.8) containing 100 mM NaCl, 2 mM MgCl₂, and 10% glycerol and stored at –80 °C until further use.

UV-Visible Spectroscopy. The binding affinities of G α -(340–350), TOAC³⁴³-G α -(340–350), and the doubly labeled Proxyl/TOAC³⁴⁸-G α -(340–350) for rhodopsin in rod outer segments (ROS) were measured using a Meta II stabilization assay (46) by UV-visible spectroscopy. The samples contained 2.5 μ M rhodopsin in ROS membranes (47) and peptides in buffer A [20 mM Tris-HCl (pH 8.0), 130 mM NaCl, 1 mM MgCl₂, and 1 μ M EDTA]. The samples were kept on ice and prepared under dim red light to avoid premature bleaching of rhodopsin. The absorption spectrum of dark-adapted rhodopsin was recorded, illuminated with 490 \pm 5 nm light for 20 s, followed by acquisition of the light-activated spectrum, using a Cary50 spectrophotometer (Varian, Palo Alto, CA). The cuvette compartment was kept at 4 $^{\circ}$ C. The measurements were taken in triplicate at varying peptide concentrations from 1 μ M to 5 mM. The Meta II stabilization was calculated as $\Delta A_{380} - \Delta A_{417}$, where ΔA is the absorbance change before and after light activation. The data were fit using the equation $MII = \text{baseline} + \text{range} \times [(\text{peptide})/(\text{peptide} + EC_{50})]$ to yield EC_{50} values of the peptides. Baseline and range values were kept constant throughout all determinations at 0.05 and 0.75, respectively.

EPR Measurements. EPR measurements were collected on a Bruker 580 spectrometer at X-band microwave frequencies using a high-sensitivity resonator (HS0118) with an optical port. Spin-labeled peptides were mixed with dark-adapted ROS in 20 mM MES buffer (pH 6.8) containing 100 mM NaCl, 2 mM MgCl₂, and 10% glycerol and loaded into a quartz flat cell. Low-affinity peptide data were recorded at 277 K to slow the disappearance of the rhodopsin-bound component (see Discussion), while high-affinity peptide data were recorded at 296 K. Spectra were initially recorded under dim red light. Samples were subsequently photobleached with a tungsten lamp (500 nm cutoff filter) for 40 s, and an EPR spectrum was recorded.

Time-resolved EPR photolysis experiments were initiated with an \sim 6 ns laser pulse (500 nm) from a Q-switched Nd:YAG laser coupled with a tunable optical paramagnetic oscillator (Vibrant, Opotek, Inc., Carlsbad, CA). The magnetic field position was set at the center field trough of the unbound peptide spectrum, and the resulting EPR transient was detected with 100 kHz field modulation. The signals were recorded with a LeCroy digital oscilloscope (LeCroy Corp., Chestnut Ridge, NY).

Double Electron-Electron Resonance (DEER) Experiments. Doubly spin-labeled peptides were mixed with dark-adapted ROS [both in 10% (v/v) glycerol] and flash-frozen in the dark in 1.5 mm \times 1.8 mm quartz capillaries in liquid nitrogen. DEER measurements were taken at 50 K on a Bruker Elexsys 580 spectrometer with a 2 mm split-ring resonator. Four-pulse DEER was conducted as previously described (7, 48) with the π pump pulse (16 ns) positioned at the absorption maximum of the field swept spectrum. The observer π (16 ns) and $\pi/2$ (8 ns) pulses were positioned at the low-field line of the spectrum ($\Delta f = 70$ MHz). After dark-state data had been acquired, the samples were thawed, illuminated with light (500 nm cutoff filter), and refrozen in liquid nitrogen for a second DEER experiment. All DEER data were analyzed with the DEER Analysis 2009 software package freely available at <http://www.epr.ethz.ch/>. Tikhonov regularization and distance distribution widths were optimized using L-curve analysis implemented in the software package.

RESULTS

Peptide Synthesis. It has been demonstrated that positions that accept Aib (α -aminobutyric acid) will usually also accept TOAC substitutions. Molecular modeling of conformationally constrained peptides identified the analogue of G α -(340–350), AibKAibAibLKDCGLG, that was synthesized and shown to maintain full activity in stabilization of the MII state of rhodopsin (49). Given that Aib mimics the conformational effect of TOAC substitutions on the peptide backbone (50–53), these results suggested that residues I340, E342, and N343 are capable of tolerating substitution. For the work outlined here, we chose substitution with TOAC at N343. A TOAC scan of the C-terminal tail also revealed that substitution of Gly348 with TOAC maintained the ability to stabilize the MII state of rhodopsin (data not shown), and doubly labeled Proxyl/TOAC³⁴⁸-G α -(340–350) was therefore prepared.

Binding of Spin-Labeled G α Peptides to Light-Activated Rhodopsin. EPR studies have focused on characterization of TOAC³⁴³-G α -(340–350) [IKE-TOAC-LKDCGLF (Figure 1D, bottom)] and the corresponding high-affinity TOAC³⁴³ analogue (VLE-TOAC-LKSVGLF) in terms of mobility in the rhodopsin-bound and unbound forms. Characterization of Proxyl³⁴⁰-G α -(340–350) (Figure 1D, top) and the corresponding high-affinity analogue has also been conducted for comparison with the TOAC analogues. The EPR spectra of the spin-labeled peptides in the presence of dark- and light-activated ROS membranes are shown in Figure 2. In each case, the spectrum of the peptide in the presence of ROS membranes in the dark is the same as that for the peptide in buffer and consists of a single component of three relatively sharp lines, characteristic of a rapidly and isotropically tumbling nitroxide (Figure 2, left). On the other hand, spectra of the peptides in the presence of photoactivated ROS membranes are a composite of two distinct components (Figure 2, center), one of which corresponds to the free peptide in solution. The other component is identified by well-resolved hyperfine extrema (arrows, Figure 2) indicative of peptide immobilization and rhodopsin binding. As expected, the amplitude of the bound component is much greater for the high-affinity analogues. The individual components, resolved by spectral subtraction, are shown for each peptide in the right panel of Figure 2. The components corresponding to the bound states (right panel, blue traces) each have line shapes characteristic of highly immobilized nitroxides. A comparison of the spectral components corresponding to the bound states reveals different mobilities for the TOAC and Proxyl analogues. An approximate rotational correlation time (τ_c) for a nitroxide may be computed from the separation of the outer hyperfine extrema ($2A_{zz}$) and that for the same sample in a frozen state in the absence of motion ($2A_{zz}^0$) (54). For the TOAC and Proxyl analogues of the high-affinity peptide bound to photoactivated rhodopsin, $2A_{zz}$ equals 69 and 64 G, respectively (Figure 2). For both analogues bound to photoactivated rhodopsin, the $2A_{zz}^0$ obtained at 223 K is 74 G (spectra not shown), indicating that the nitroxides in each case are located in a polar environment, presumably facing the solvent. From these values, assuming Brownian motion, τ_c is estimated to be 19.4 and 8.7 ns for the TOAC and Proxyl analogues, respectively. Thus, the TOAC analogue of the high-affinity peptide is more immobilized than the corresponding Proxyl analogue. Because the rotational diffusion of rhodopsin in the disk is very slow [$\tau_R \approx 12$ μ s (55)] and because TOAC is rigidly attached to the peptide backbone, the 19.4 ns correlation time for the TOAC analogue directly

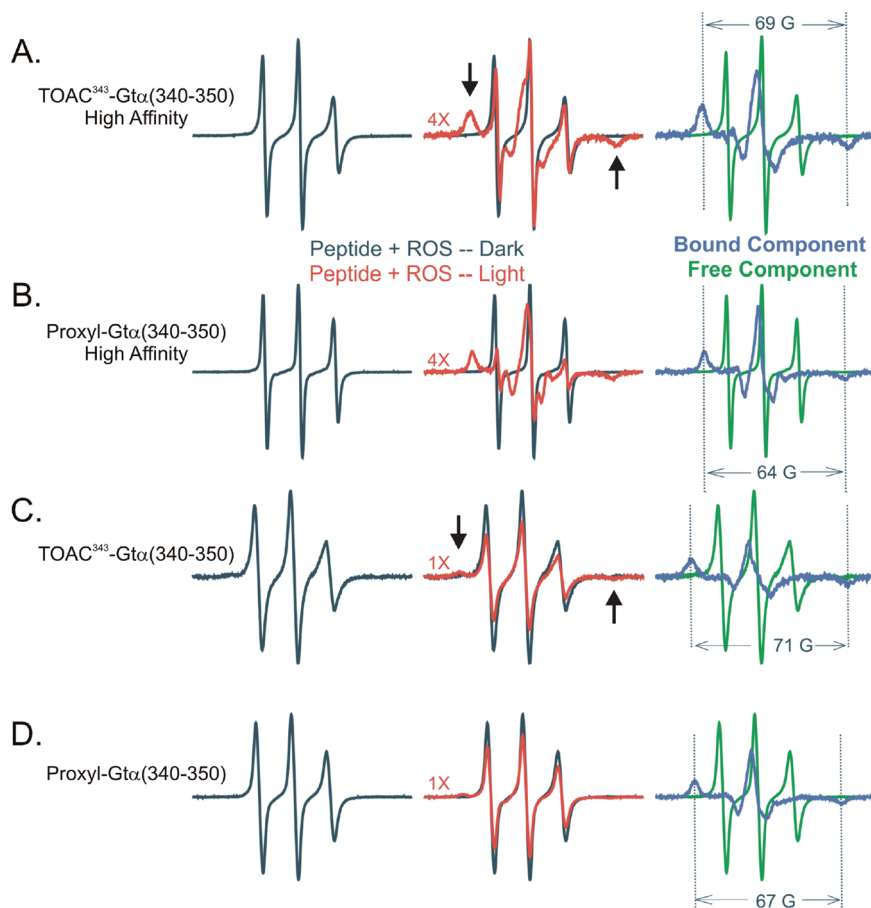


FIGURE 2: EPR spectra of the indicated spin-labeled peptides: (left) spectra in the presence of dark-adapted ROS membranes, (center) spectra in the presence of photoactivated ROS membranes (red trace) compared to those in the dark-adapted state (black trace), and (right) spectra of the pure bound (blue trace) and unbound (green trace) states obtained by spectral subtraction. The high-affinity peptide data were recorded with a 2 G modulation amplitude at 296 K. The low-affinity TOAC³⁴³-Gtα(340–350) and Proxyl-Gtα(340–350) peptide data were recorded with a 4 G modulation amplitude at 277 K to facilitate detection of the bound component. The higher modulation accounts for the broader lines in the spectra of the unbound component in panels C and D. EPR spectra in the left and center panels have been normalized to the same number of spins and plotted with the indicated scaling factor. Individual component spectra (right) are arbitrarily scaled for direct line shape comparison. The samples were in 20 mM MES buffer (pH 6.8) containing 100 mM NaCl, 2 mM MgCl₂, and 10% glycerol.

measures the fluctuation frequency of the peptide in the rhodopsin binding site. Differences in $2A_{zz}$ and hence mobility are observed between TOAC and Proxyl in both the low- and high-affinity peptides.

Activity of the Peptides: Stabilization of MII. The binding of a C-terminal Gtα peptide or analogue to photoactivated rhodopsin can be monitored by an increase in the amount of MII due to the presence of the peptide. A dose–response curve of the peptide concentration relative to its effect on MII stabilization can be fit to the model described in Materials and Methods to provide a value for the apparent dissociation constant (K_d). Results are compared for the native Gtα(340–350), TOAC³⁴³-Gtα(340–350), and Proxyl-Gtα(340–350) in Figure 1E. The data reveal that the presence of the TOAC³⁴³ or Proxyl group has little effect on the binding affinity for the receptor. Figure 3B shows examples for the TOAC³⁴³-Gtα(340–350) high-affinity peptide compared with the high-affinity peptide without TOAC. The fits to the data, shown by the solid traces, give K_d values of 10 and 4.2 μ M, respectively. Thus, the presence of the TOAC spin-label at position 343 increases the K_d by a factor of ≈ 2.5 , corresponding to a modest increase in the free energy of the bound state by 0.5 kcal/mol due to the TOAC.

It is of interest to compare the apparent dissociation constant for a spin-labeled peptide determined by the MII stabilization

assay with that determined from direct binding using EPR. The left panel of Figure 3A shows the absorption EPR spectrum (obtained by integration of the first-derivative spectra) corresponding to the equilibrium of the TOAC³⁴³-Gtα(340–350) high-affinity peptide with photoactivated rhodopsin (black trace). Also shown are the individual components corresponding to the bound and free peptide (red and green traces, respectively), obtained by subtraction. Integration of the individual spectra provides the relative equilibrium concentrations of each, which gives a K_d of 12.5 μ M for the TOAC³⁴³-Gtα(340–350) high-affinity peptide. This compares favorably with the value of 10 μ M obtained from the MII stabilization data shown in Figure 3B. The right panel of Figure 3A shows similar data for the Proxyl-Gtα(340–350) high-affinity peptide, giving a K_d of 4 μ M. This value is essentially identical to that obtained for the nonlabeled high-affinity analogue using the MII stabilization assay, suggesting that the terminal location of the spin-label does not perturb the peptide–R* interaction. Interestingly, the peptide dissociation constants measured in Figure 3A via EPR techniques did not vary over a pH range of 6–8 (data not shown).

Kinetics of Binding for Gtα Peptide Analogues. The kinetics of binding to photoactivated rhodopsin (R*) for the TOAC³⁴³-Gtα(340–350) high-affinity peptide was determined by monitoring the EPR signal after a ~ 6 ns actinic flash at 500 nm. Figure 4A

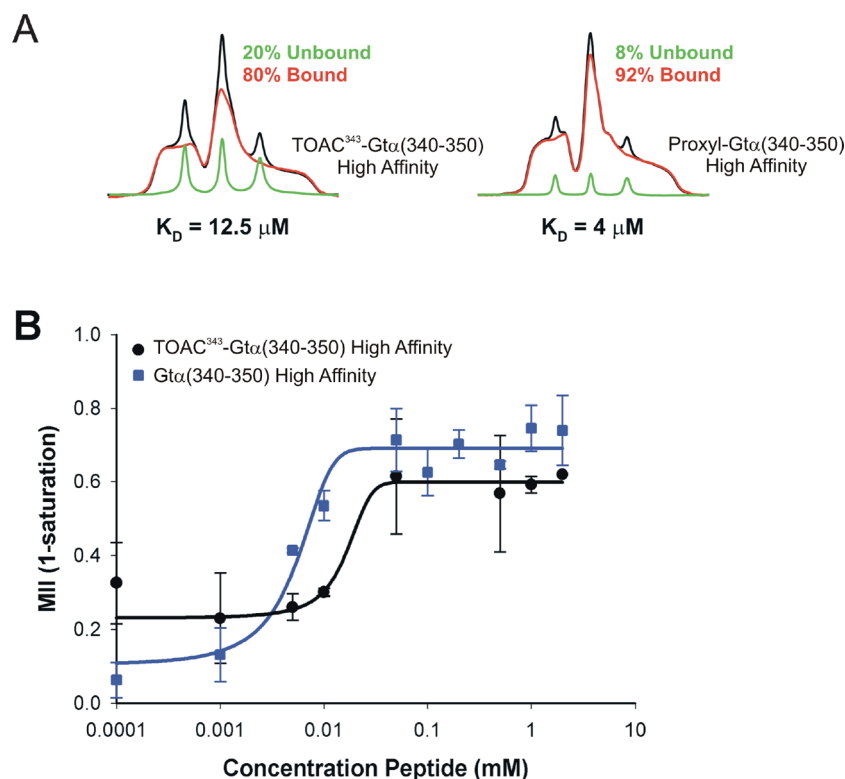


FIGURE 3: Binding of the high-affinity spin-labeled peptides to photoactivated rhodopsin. (A) Absorption EPR spectra for the TOAC and Proxyl high-affinity peptides in equilibrium with photoactivated rhodopsin at 296 K. The composite absorption spectra (black lines) are shown with the individual spectral components overlaid in green and red. The percentage of rhodopsin-bound peptide was determined by spectral integration. The concentrations of rhodopsin and spin-labeled peptide were 90 and 50 μM, respectively. The samples were in 20 mM MES buffer (pH 6.8) containing 100 mM NaCl, 2 mM MgCl₂, and 10% glycerol. (B) Dose responses of MII formation to determine K_d values for TOAC³⁴³-Gtα(340–350) and Gtα(340–350) high-affinity peptides. The measurements were taken independently with different preparation of ROS, and the graphs were not normalized to overlap initial and final values.

shows the EPR spectral amplitude recorded at three different peptide concentrations (gray, green, and red traces) monitored at the centerfield trough of the EPR spectrum, corresponding to the unbound peptide (see Figure 2A, right). Data were collected as a function of time after the laser pulse and fit to a single-exponential rise (black line) with an apparent lifetime of ~6 ms. The time course of peptide binding was independent of the peptide concentration for the three concentrations tested, suggesting that the binding event is rate-limited by structural changes within the rhodopsin photoreceptor that lead to opening of the binding site rather than diffusion of the peptide to the receptor. The data were collected under either pseudo-first-order (2.5 mM peptide) or second-order (50 and 250 μM peptide) conditions. The second-order reaction, however, is not a simple second-order binding event but instead is coupled to the unimolecular appearance of the active receptor state. Figure 4B shows EPR absorption spectra collected as a function of time after the initial rapid binding event. As is evident, the broad spectral component, corresponding to the bound peptide, decreases in time with a concomitant increase in the sharp component, reflecting a slow, spontaneous, dissociation of the bound peptide from R*. The decay of the bound signal can be fit with a single exponential with a half-life of 8 min [Figure 4D (○)], similar to that for MII decay in native disk membranes (56).

Similar results were obtained for the dissociation of the Proxyl-Gtα(340–350) high-affinity peptide from R* (Figure 4C), and the data are included in the plot of Figure 4D (triangles). These results further demonstrate the functionality of the spin-labeled Gtα(340–350) analogues in their ability to bind and stabilize R* and to sense the activated conformational state of the receptor.

DEER Spectroscopy. To investigate the conformation of the peptide bound to MII, the high-affinity analogue of doubly labeled Proxyl/TOAC³⁴⁸-Gtα(340–350) (Figure 5A) was prepared so that the distribution of interspin distances in the peptide (in solution or when bound to R*) could be monitored by DEER spectroscopy. The K_d of this peptide was 65 μM, and as expected, the EPR spectra of the unbound and bound peptides reflected rapid isotropic motion and strong immobilization, respectively, similar to the spectra of the peptides containing a single nitroxide (Figure 5B). The featureless dipolar evolution function of the peptide in the presence of dark rhodopsin (Figure 5C, top trace) and the corresponding dipolar spectrum (Figure 5D, black trace) reflect a broad distribution of inter-nitroxide distances in the range 18–34 Å (Figure 5E, black trace), consistent with an ensemble of conformations for the unbound peptide. Distance distributions of peaks longer than 34 Å in Figure 5E are inaccurately determined because of the 1.1 μs length of the dipolar evolution functions. On the other hand, in the presence of R*, striking oscillations are evident in the dipolar evolution function (Figure 5C, bottom trace) corresponding to a remarkably narrow interspin distance distribution centered at 19 Å (Figure 5E, red trace). Modeling of the nitroxides in the crystal structure conformation of the peptide (41) (Figure 5F) shows this distance to be consistent with the crystal structure and the unique configuration of the R*-bound Gtα(340–350) as determined by Kisselev et al. from NMR (39).

DISCUSSION

Heterotrimeric α subunits have been shown to have several contact regions that are critical for receptor interaction (19, 57).

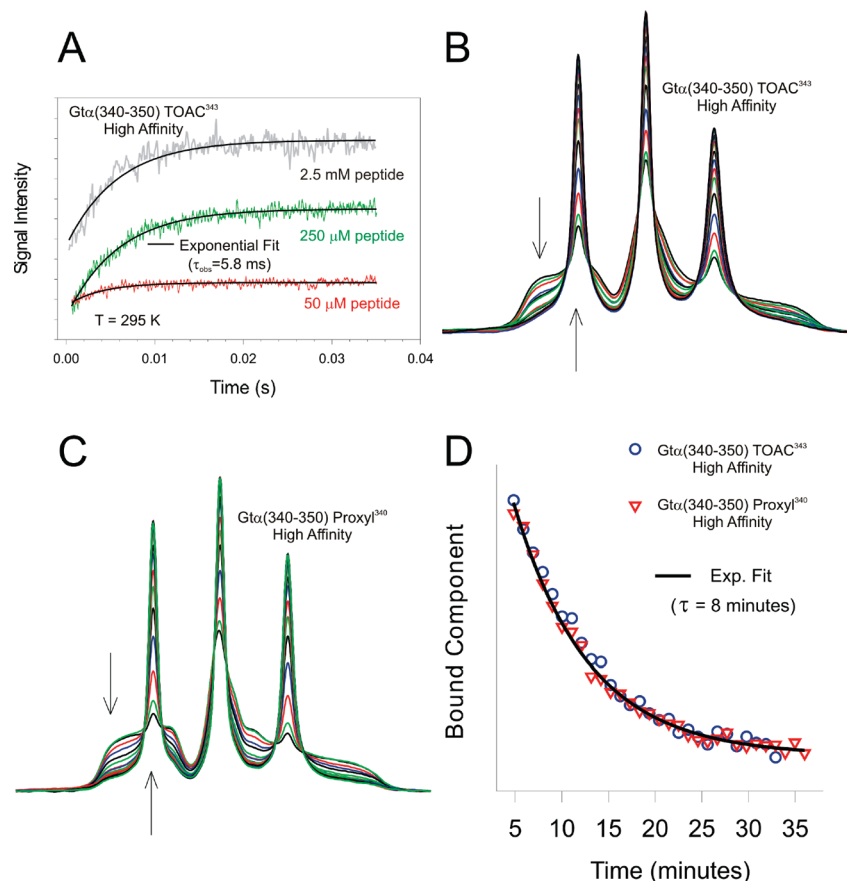


FIGURE 4: Binding and dissociation kinetics for high-affinity spin-labeled peptides. (A) Transient EPR changes for the TOAC³⁴³-Gtα(340–350) high-affinity peptide collected at the centerfield trough of the free peptide spectrum are plotted as a function of time after the laser flash. The gray, green, and red traces were collected at peptide concentrations of 2.5 mM, 250 μM, and 50 μM, respectively. The rhodopsin concentration was 250 μM. The samples were in 20 mM MES buffer (pH 6.8) containing 100 mM NaCl, 2 mM MgCl₂, and 10% glycerol. All three traces were well fit with a single-exponential function with a lifetime of 5.8 ms (black solid lines). (B) EPR absorption spectra as a function of time following the rapid transient showing the decay of the immobile spectral component and the appearance of a mobile species for the TOAC³⁴³-Gtα(340–350) high-affinity peptide and (C) for Proxyl-Gtα(340–350) high-affinity peptides. The arrows indicate the direction of the line shape changes over time. (D) Decay of the bound component with time: (blue circles) TOAC³⁴³-Gtα(340–350) high-affinity peptides and (red triangles) Proxyl-Gtα(340–350) high-affinity peptides. A single exponential (black line) with a time constant of 8 min was fit to the data.

One of these regions is apparently the C-terminal sequence of Gtα, as shown by the fact that a synthetic undecapeptide corresponding to Gtα(340–350) binds to R* and stabilizes the MII state, thus mimicking the effects of transducin itself (37).

In this study, we provide evidence that five spin-labeled Gtα(340–350) analogues maintain their ability to bind and stabilize the photoactivated MII state of rhodopsin. Receptor binding was detected by immobilization of incorporated TOAC and Proxyl residues as the peptide adopts a highly restricted bound conformation. Comparison between the peptide analogues revealed a higher degree of immobilization with the TOAC than the Proxyl analogue. The difference in immobilization can be explained in part by the fact that the N-terminal Proxyl label is connected by an amide linkage to the Gtα(340–350) backbone and thus potentially has two additional rotational degrees of freedom relative to TOAC. TOAC is incorporated directly within the peptide chain and has only limited internal motion relative to the backbone. Hence, when the peptide is immobilized on R*, so is the TOAC nitroxide. Interestingly, however, there is some degree of motion on the nanosecond time scale still present in the bound TOAC³⁴³-Gtα(340–350) and high-affinity analogue that cannot be attributed to R* rotational diffusion. The rotational correlation time of rhodopsin in native disk membranes has been measured to be 20–40 μs (58, 59). This motion is too slow to affect

the EPR line shape, which is sensitive to motion in the 100 ps to 100 ns time domain. Thus, the nanosecond motions detected in the bound peptide reflect structural fluctuations of the peptide in the binding site on this time scale. It should be possible to construct approximate partition functions from the distance distributions seen in Figure 5 to estimate the change in entropy of the peptide ligand on binding to photoactivated rhodopsin.

Consistent with the conformation of Gtα(340–350) peptides bound to R* observed by NMR is the crystal structure of the complex of opsin with this undecapeptide (41). The crystal structure helps to further rationalize the differences in nitroxide rotational correlation times of the Proxyl and TOAC adducts (see above). Models of the Proxyl peptide using the crystallographic data show that this label projects outward toward solvent (see Figure 5F). Motion due to the additional rotational degrees of freedom is consistent with the higher mobility of the Proxyl relative to the TOAC nitroxide. Note, however, that the Proxyl is still quite immobilized, presumably due to contacts of the nitroxide ring with nearby side chains in rhodopsin. The TOAC³⁴³-Gtα(340–350) peptide is also solvent accessible (model not shown), but the internal constraints of this spin-label prevent additional nitroxide motion. Finally, a TOAC label placed at position 348 reduced the affinity of the labeled peptide (see Figure 5B), likely because the TOAC-348 residue is predicted to

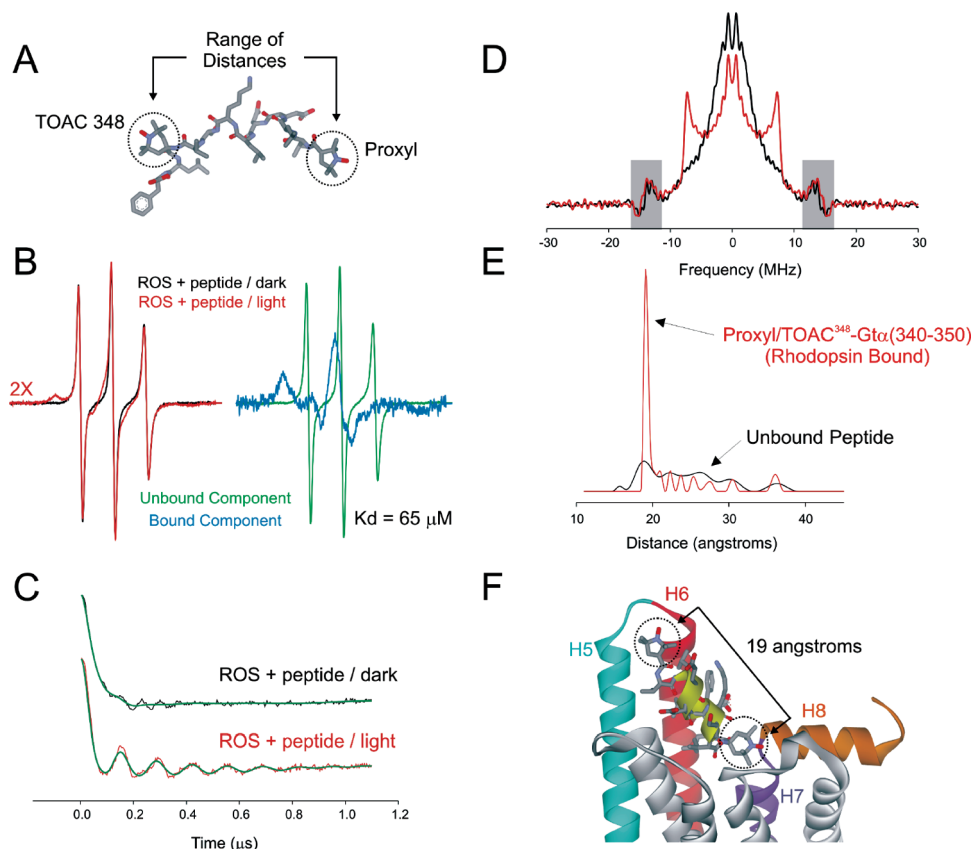


FIGURE 5: DEER distance measurements for the doubly spin-labeled peptide Proxyl/TOAC³⁴⁸-Gtα(340–350). (A) Diagram of the high-affinity doubly labeled undecapeptide. A range of distances between spin-labels was anticipated for the unbound peptide in solution. (B) Estimation of the dissociation constant of the peptide. EPR spectrum of 90 μ M ROS mixed with 50 μ M peptide before (black trace) and after (red trace) photobleaching. The individual spectral components were obtained as described above, and a K_d of 65 μ M was determined. The samples were in 20 mM MES buffer (pH 6.8) containing 100 mM NaCl, 2 mM MgCl₂, and 10% glycerol. (C) Dipolar evolution functions for the unbound (black trace) and rhodopsin-bound (red trace) peptide. The ROS and peptide concentrations were 250 and 200 μ M, respectively. The green traces represent fits to the data using Tikhonov regularization as implemented in the DEER Analysis 2009 software package (see Materials and Methods). The high-frequency oscillations observed in the unbound peptide dipolar evolution function are electron/proton ESEEM signals that are not fit using the DEER Analysis software package. (D) Dipolar spectra of the unbound (black trace) and rhodopsin-bound (red trace) peptide. The gray highlighted regions indicate frequencies at which ESEEM signals appear. (E) Distance distributions for the unbound (black trace) and rhodopsin-bound (red trace) peptide. (F) Model of the rhodopsin-bound doubly labeled Proxyl/TOAC³⁴⁸-Gtα(340–350) high-affinity peptide based on the peptide-bound crystal structure of opsin (39). Helices 5–8 in opsin are colored cyan, red, purple, and orange, respectively. The peptide ribbon is colored yellow, while side chains are shown as sticks. The distance as measured by DEER between the two spin-labels matched that predicted from NMR structural data (model not shown) as well as the peptide-bound crystal structure of opsin (39). The Proxyl side chain is more solvent-exposed and is projected toward the helix 5–helix 6 loop in opsin, while TOAC-348 is buried near the helix 7–helix 8 interface. Steric contacts between TOAC-348 and opsin likely reduce its binding affinity relative to other spin-labeled peptides [K_d {Proxyl/TOAC³⁴⁸-Gtα(340–350)} = 65 μ M].

have steric clashes with the receptor near the helix 7–helix 8 region (see Figure 5F).

Studies of the kinetics of a peptide binding to a cognate receptor are an important strategy for exploring the mechanism of protein–protein recognition. The kinetics of binding of Gtα(340–350) and the high-affinity analogue to R* have been previously investigated at a low temperature (1.5 °C) and a high pH (7.9) by monitoring the production of “extra MII” induced by peptide binding (60). An advantage of the EPR method described here is that it is a direct measure of the binding interaction compared to the extra Meta II assay which relies upon changes in chromophore protonation states at a receptor site distant from the receptor–G-protein interface. In addition, physiological temperatures, a wide range of pH values, and high concentrations of native disk membranes can be used in the EPR method to investigate the binding mechanism. The latter point is raised because light scattering artifacts due to a high concentration of membrane vesicles can complicate interpretation of optical signals but present no problem in magnetic resonance detection.

Light scattering methods have also been used to measure peptide binding to R*, but this method requires an increase in the mass of the peptide, accomplished by fusing the peptide to maltose binding protein (MBP, 42.5 kDa) (61). While these fused peptides were shown to bind to rhodopsin in a light-dependent manner, rate data were likely influenced by the presence of MBP due to changes in the diffusion constant and, most importantly, to steric constraints on the binding event. It could be argued that the presence of the spin-label in the peptide could also modify the binding kinetics, but the similarity of the K_d for the singly labeled and native peptides suggests otherwise.

As shown by the data in Figure 4, the rate of peptide binding to R* as measured by EPR follows a single-exponential time course that is apparently rate-limited by conformational changes in rhodopsin that lead to the binding competent state of the receptor. This is consistent with earlier studies which showed fast proton release within rhodopsin upon formation of the peptide–receptor complex (16) in DM micelles. The proton release was rate limited by the appearance of the active receptor state at reagent

concentrations much lower than those used in our work, verifying the validity of the rate-limiting step approximation. The time constant for binding to rhodopsin in ROS membranes observed here (≈ 6 ms) is in the time window for formation of deprotonated forms of the receptor detected optically at 380 nm (MIIa, MIIb, and MIIbH⁺) (62–64); presumably, the binding competent state corresponds to one of these intermediates. SDSL data first provided direct evidence that the outward movement of transmembrane helix 6 (TM6) by ~ 5 Å gives rise to the activated state of the receptor (18, 65). The outward movement of TM6 is consistent with generation of a binding pocket for the C-terminal tail of the G α subunit (and the corresponding peptides) within the intracellular loops of R*. This model is directly supported by the recent crystal structure of an opsin–G α (340–350) peptide (41). It is thus reasonable to speculate that the peptide binding is rate-limited by the movement of TM6. The time constant for TM6 movement following an activating light flash has in fact been measured by SDSL to be ≈ 2 ms and was shown to correspond to the formation of MIIb, but this was determined for rhodopsin in micelles of DM where rate constants for interconversion of the intermediates are generally accelerated (16). Future studies will be required to identify the specific intermediate competent for peptide binding in the native membrane.

The ability to synthesize fully active, TOAC-labeled analogues of G α (340–350) provides a strategy for mapping the structure of the rhodopsin–peptide complex using distance measurements between pairs of spins, one in the peptide and the other at selected sites throughout the cytoplasmic domain of rhodopsin. Such measurements will determine the relative orientation and position of the bound peptide within the complex and may identify any additional lower-affinity binding modes. The TOAC spin-label is ideally suited for this purpose, because incorporation of α , β , and γ carbons as well as the nitroxide moiety into one heterocyclic structure eliminates rotation about side chain bonds, effectively fixing the nitroxide relative to the backbone. This is a significant advantage over the more commonly used nitroxide side chains where the possible existence of multiple rotamers complicates the interpretation of interspin distances.

Incorporation of synthetic peptides into a G α subunit by expressed protein ligation has been demonstrated (66, 67), setting the stage for future studies that incorporate a TOAC-labeled G α (340–350) peptide into the full-length G α . Thus, it would be possible to compare salient structural features of the complex formed with R* by the isolated peptide with that formed by the full-length G α . Such studies using the internally constrained TOAC should be able to measure structural heterogeneity at the rhodopsin–transducin interface and explore the effect of allosteric regulators. Such studies should provide insight into enzymatic mechanisms of transducin activation by R*.

REFERENCES

- Hubbell, W. L., Gross, A., Langen, R., and Lietzow, M. A. (1998) Recent advances in site-directed spin labeling of proteins. *Curr. Opin. Struct. Biol.* 8, 649–656.
- Hubbell, W. L., Cafiso, D. S., and Altenbach, C. (2000) Identifying conformational changes with site-directed spin labeling. *Nat. Struct. Biol.* 7, 735–739.
- Columbus, L., and Hubbell, W. L. (2002) A new spin on protein dynamics. *Trends Biochem. Sci.* 27, 288–295.
- Rabenstein, M. D., and Shin, Y. K. (1995) Determination of the distance between two spin labels attached to a macromolecule. *Proc. Natl. Acad. Sci. U.S.A.* 92, 8239–8243.
- Altenbach, C., Oh, K. J., Trabanino, R. J., Hideg, K., and Hubbell, W. L. (2001) Estimation of inter-residue distances in spin labeled proteins at physiological temperatures: Experimental strategies and practical limitations. *Biochemistry* 40, 15471–15482.
- Jeschke, G. (2002) Distance measurements in the nanometer range by pulse EPR. *ChemPhysChem* 3, 927–932.
- Pannier, M., Veit, S., Godt, A., Jeschke, G., and Spiess, H. W. (2000) Dead-time free measurement of dipole-dipole interactions between electron spins. *J. Magn. Reson.* 142, 331–340.
- Langen, R., Oh, K. J., Cascio, D., and Hubbell, W. L. (2000) Crystal structures of spin labeled T4 lysozyme mutants: Implications for the interpretation of EPR spectra in terms of structure. *Biochemistry* 39, 8396–8405.
- Fleissner, M. R., Cascio, D., and Hubbell, W. L. (2009) Structural origin of weakly ordered nitroxide motion in spin-labeled proteins. *Protein Sci.* 18, 893–908.
- Guo, Z., Cascio, D., Hideg, K., and Hubbell, W. L. (2008) Structural determinants of nitroxide motion in spin-labeled proteins: Solvent-exposed sites in helix B of T4 lysozyme. *Protein Sci.* 17, 228–239.
- Guo, Z., Cascio, D., Hideg, K., Kalai, T., and Hubbell, W. L. (2007) Structural determinants of nitroxide motion in spin-labeled proteins: tertiary contact and solvent-inaccessible sites in helix G of T4 lysozyme. *Protein Sci.* 16, 1069–1086.
- McHaourab, H. S., Lietzow, M. A., Hideg, K., and Hubbell, W. L. (1996) Motion of spin-labeled side chains in T4 lysozyme. Correlation with protein structure and dynamics. *Biochemistry* 35, 7692–7704.
- Lietzow, M. A., and Hubbell, W. L. (2004) Motion of spin label side chains in cellular retinol-binding protein: Correlation with structure and nearest-neighbor interactions in an antiparallel β -sheet. *Biochemistry* 43, 3137–3151.
- Columbus, L., Kalai, T., Jeko, J., Hideg, K., and Hubbell, W. L. (2001) Molecular motion of spin labeled side chains in α -helices: Analysis by variation of side chain structure. *Biochemistry* 40, 3828–3846.
- Steinhoff, H. J., Mollaaghabaga, R., Altenbach, C., Hideg, K., Krebs, M., Khorana, H. G., and Hubbell, W. L. (1994) Time-resolved detection of structural changes during the photocycle of spin-labeled bacteriorhodopsin. *Science* 266, 105–107.
- Knierim, B., Hofmann, K. P., Ernst, O. P., and Hubbell, W. L. (2007) Sequence of late molecular events in the activation of rhodopsin. *Proc. Natl. Acad. Sci. U.S.A.* 104, 20290–20295.
- Hubbell, W. L., Altenbach, C., Hubbell, C. M., and Khorana, H. G. (2003) Rhodopsin structure, dynamics, and activation: A perspective from crystallography, site-directed spin labeling, sulfhydryl reactivity, and disulfide cross-linking. *Adv. Protein Chem.* 63, 243–290.
- Altenbach, C., Kusnetzow, A. K., Ernst, O. P., Hofmann, K. P., and Hubbell, W. L. (2008) High-resolution distance mapping in rhodopsin reveals the pattern of helix movement due to activation. *Proc. Natl. Acad. Sci. U.S.A.* 105, 7439–7444.
- Oldham, W. M., Van Eps, N., Preininger, A. M., Hubbell, W. L., and Hamm, H. E. (2007) Mapping allosteric connections from the receptor to the nucleotide binding pocket of heterotrimeric G proteins. *Proc. Natl. Acad. Sci. U.S.A.* 104, 7927–7932.
- Van Eps, N., Oldham, W. M., Hamm, H. E., and Hubbell, W. L. (2006) Structural and dynamical changes in an α -subunit of a heterotrimeric G protein along the activation pathway. *Proc. Natl. Acad. Sci. U.S.A.* 103, 16194–16199.
- Oldham, W. M., Van Eps, N., Preininger, A. M., Hubbell, W. L., and Hamm, H. E. (2006) Mechanism of the receptor-catalyzed activation of heterotrimeric G proteins. *Nat. Struct. Mol. Biol.* 13, 772–777.
- Preininger, A. M., Van Eps, N., Yu, N. J., Medkova, M., Hubbell, W. L., and Hamm, H. E. (2003) The myristoylated amino terminus of G α_{i1} plays a critical role in the structure and function of G α_{i1} subunits in solution. *Biochemistry* 42, 7931–7941.
- Medkova, M., Preininger, A. M., Yu, N. J., Hubbell, W. L., and Hamm, H. E. (2002) Conformational changes in the amino-terminal helix of the G protein α_{i1} following dissociation from G $\beta\gamma$ subunit and activation. *Biochemistry* 41, 9962–9972.
- Hurth, K. M., Nilges, M. J., Carlson, K. E., Tamrazi, A., Belford, R. L., and Katzenellenbogen, J. A. (2004) Ligand-induced changes in estrogen receptor conformation as measured by site-directed spin labeling. *Biochemistry* 43, 1891–1907.
- Rassat, A., and Rey, P. (1967) Nitroxides. XXIII. Preparation d'amino-acides radicalaires et de leurs sels complexes. *Bull. Soc. Chim. Fr.*, 815.
- Marsh, D. (2006) Orientation of TOAC amino-acid spin labels in α -helices and β -strands. *J. Magn. Reson.* 180, 305–310.
- Crisma, M., Deschamps, J. R., George, C., Flippen-Anderson, J. L., Kaptein, B., Broxterman, Q. B., Moretto, A., Oancea, S., Jost, M., Formaggio, F., and Toniolo, C. (2005) A topographically and conformationally constrained, spin-labeled, α -amino acid: Crystallographic characterization in peptides. *J. Pept. Res.* 65, 564–579.

28. Schiemann, O., Cekan, P., Margraf, D., Prisner, T. F., and Sigurdsson, S. T. (2009) Relative orientation of rigid nitroxides by PELDOR: Beyond distance measurements in nucleic acids. *Angew. Chem., Int. Ed.* **48**, 3292–3295.
29. Barbosa, S. R., Cilli, E. M., Lamy-Freund, M. T., Castrucci, A. M., and Nakaie, C. R. (1999) First synthesis of a fully active spin-labeled peptide hormone. *FEBS Lett.* **446**, 45–48.
30. Vesterman, B., Sekacis, I., Betins, J., Podins, L., and Nikiforovich, G. V. (1985) Equilibrium of conformers in solution: Spin-labelled angiotensin. *FEBS Lett.* **192**, 128–130.
31. Nakaie, C. R., Silva, E. G., Cilli, E. M., Marchetto, R., Schreier, S., Paiva, T. B., and Paiva, A. C. (2002) Synthesis and pharmacological properties of TOAC-labeled angiotensin and bradykinin analogs. *Peptides* **23**, 65–70.
32. Bettio, A., Gutewort, V., Poppl, A., Dinger, M. C., Zschornig, O., Klaus, A., Toniolo, C., and Beck-Sickinger, A. G. (2002) Electron paramagnetic resonance backbone dynamics studies on spin-labelled neuropeptide Y analogues. *J. Pept. Sci.* **8**, 671–682.
33. Smythe, M. L., Nakaie, C. R., and Marshall, G. R. (1995) α -Helical versus 3_{10} -Helical Conformation of Alanine-Based Peptides in Aqueous Solution: An Electron Spin Resonance Investigation. *J. Am. Chem. Soc.* **117**, 10555–10562.
34. Hanson, P., Martinez, G., Millhauser, G., Formaggio, F., Crisma, M., Toniolo, C., and Vita, C. (1996) Distinguishing Helix Conformations in Alanine-Rich Peptides Using the Unnatural Amino Acid TOAC and Electron Spin Resonance. *J. Am. Chem. Soc.* **118**, 271–272.
35. Emeis, D., Kuhn, H., Reichert, J., and Hofmann, K. P. (1982) Complex formation between metarhodopsin II and GTP-binding protein in bovine photoreceptor membranes leads to a shift of the photoproduct equilibrium. *FEBS Lett.* **143**, 29–34.
36. Sakmar, T. P. (1998) Rhodopsin: A prototypical G protein-coupled receptor. *Prog. Nucleic Acid Res. Mol. Biol.* **59**, 1–34.
37. Hamm, H. E., Deretic, D., Arendt, A., Hargrave, P. A., Koenig, B., and Hofmann, K. P. (1988) Site of G protein binding to rhodopsin mapped with synthetic peptides from the α subunit. *Science* **241**, 832–835.
38. Dratz, E. A., Furstenau, J. E., Lambert, C. G., Thireault, D. L., Rarick, H., Schepers, T., Pakhlevanians, S., and Hamm, H. E. (1993) NMR structure of a receptor-bound G-protein peptide. *Nature* **363**, 276–281.
39. Kisselev, O. G., Kao, J., Ponder, J. W., Fann, Y. C., Gautam, N., and Marshall, G. R. (1998) Light-activated rhodopsin induces structural binding motif in G protein α subunit. *Proc. Natl. Acad. Sci. U.S.A.* **95**, 4270–4275.
40. Koenig, B. W., Kontaxis, G., Mitchell, D. C., Louis, J. M., Litman, B. J., and Bax, A. (2002) Structure and orientation of a G protein fragment in the receptor bound state from residual dipolar couplings. *J. Mol. Biol.* **322**, 441–461.
41. Scheerer, P., Park, J. H., Hildebrand, P. W., Kim, Y. J., Krauss, N., Choe, H. W., Hofmann, K. P., and Ernst, O. P. (2008) Crystal structure of opsin in its G-protein-interacting conformation. *Nature* **455**, 497–502.
42. Yang, C. S., Skiba, N. P., Mazzoni, M. R., and Hamm, H. E. (1999) Conformational changes at the carboxyl terminus of G α occur during G protein activation. *J. Biol. Chem.* **274**, 2379–2385.
43. Oldham, W. M., Van Eps, N., Preininger, A. M., Hubbell, W. L., and Hamm, H. E. (2006) Mechanism of the receptor-catalyzed activation of heterotrimeric G proteins. *Nat. Struct. Mol. Biol.* **13**, 772–777.
44. Martin, E. L., Rens-Domiano, S., Schatz, P. J., and Hamm, H. E. (1996) Potent peptide analogues of a G protein receptor-binding region obtained with a combinatorial library. *J. Biol. Chem.* **271**, 361–366.
45. Mazzoni, M. R., Malinski, J. A., and Hamm, H. E. (1991) Structural analysis of rod GTP-binding protein, Gt. Limited proteolytic digestion pattern of Gt with four proteases defines monoclonal antibody epitope. *J. Biol. Chem.* **266**, 14072–14081.
46. Kisselev, O., Ermolaeva, M., and Gautam, N. (1995) Efficient interaction with a receptor requires a specific type of prenyl group on the G protein γ subunit. *J. Biol. Chem.* **270**, 25356–25358.
47. Papermaster, D. S., and Dreyer, W. J. (1974) Rhodopsin content in the outer segment membranes of bovine and frog retinal rods. *Biochemistry* **13**, 2438–2444.
48. Hanson, S. M., Van Eps, N., Francis, D. J., Altenbach, C., Vishnivetskiy, S. A., Arshavsky, V. Y., Klug, C. S., Hubbell, W. L., and Gurevich, V. V. (2007) Structure and function of the visual arrestin oligomer. *EMBO J.* **26**, 1726–1736.
49. Arimoto, R., Kisselev, O. G., Makara, G. M., and Marshall, G. R. (2001) Rhodopsin-transducin interface: Studies with conformationally constrained peptides. *Biophys. J.* **81**, 3285–3293.
50. Monaco, V., Formaggio, F., Crisma, M., Toniolo, C., Hanson, P., Millhauser, G., George, C., Deschamps, J. R., and Flippen-Anderson, J. L. (1999) Determining the occurrence of a 3_{10} -helix and an α -helix in two different segments of a lipopeptaibol antibiotic using TOAC, a nitroxide spin-labeled C α -tetrasubstituted α -amino acid. *Bioorg. Med. Chem.* **7**, 119–131.
51. Toniolo, C., Valente, E., Formaggio, F., Crisma, M., Pilloni, G., Corvaja, C., Toffoletti, A., Martinez, G. V., Hanson, M. P., and Millhauser, G. L.; et al. (1995) Synthesis and conformational studies of peptides containing TOAC, a spin-labelled C α , α -disubstituted glycine. *J. Pept. Sci.* **1**, 45–57.
52. Monaco, V., Formaggio, F., Crisma, M., Toniolo, C., Hanson, P., and Millhauser, G. L. (1999) Orientation and immersion depth of a helical lipopeptaibol in membranes using TOAC as an ESR probe. *Biopolymers* **50**, 239–253.
53. McNulty, J. C., Silapiew, J. L., Carnevali, M., Farrar, C. T., Griffin, R. G., Formaggio, F., Crisma, M., Toniolo, C., and Millhauser, G. L. (2000) Electron spin resonance of TOAC labeled peptides: Folding transitions and high frequency spectroscopy. *Biopolymers* **55**, 479–485.
54. Freed, J. H. (1976) in *Spin Labeling: Theory and Application* (Berliner, L. J., Ed.) pp 53–132, Academic Press, New York.
55. Cone, R. A. (1972) Rotational diffusion of rhodopsin in the visual receptor membrane. *Nat. New Biol.* **236**, 39–43.
56. Heck, M., Schadel, S. A., Maretzki, D., Bartl, F. J., Ritter, E., Palczewski, K., and Hofmann, K. P. (2003) Signaling states of rhodopsin. Formation of the storage form, metarhodopsin III, from active metarhodopsin II. *J. Biol. Chem.* **278**, 3162–3169.
57. Johnston, C. A., and Siderovski, D. P. (2007) Structural basis for nucleotide exchange on G α i subunits and receptor coupling specificity. *Proc. Natl. Acad. Sci. U.S.A.* **104**, 2001–2006.
58. Kusumi, A., and Hyde, J. S. (1982) Spin-label saturation-transfer electron spin resonance detection of transient association of rhodopsin in reconstituted membranes. *Biochemistry* **21**, 5978–5983.
59. Downer, N. W., and Cone, R. A. (1985) Transient dichroism in photoreceptor membranes indicates that stable oligomers of rhodopsin do not form during excitation. *Biophys. J.* **47**, 277–284.
60. Kisselev, O. G., Meyer, C. K., Heck, M., Ernst, O. P., and Hofmann, K. P. (1999) Signal transfer from rhodopsin to the G-protein: Evidence for a two-site sequential fit mechanism. *Proc. Natl. Acad. Sci. U.S.A.* **96**, 4898–4903.
61. Herrmann, R., Heck, M., Henklein, P., Kleuss, C., Hofmann, K. P., and Ernst, O. P. (2004) Sequence of interactions in receptor-G protein coupling. *J. Biol. Chem.* **279**, 24283–24290.
62. Arnis, S., and Hofmann, K. P. (1993) Two different forms of metarhodopsin II: Schiff base deprotonation precedes proton uptake and signaling state. *Proc. Natl. Acad. Sci. U.S.A.* **90**, 7849–7853.
63. Mah, T. L., Szundi, I., Lewis, J. W., Jager, S., and Kliger, D. S. (1998) The effects of octanol on the late photointermediates of rhodopsin. *Photochem. Photobiol.* **68**, 762–770.
64. Lewis, J. W., Szundi, I., Kazmi, M. A., Sakmar, T. P., and Kliger, D. S. (2006) Proton movement and photointermediate kinetics in rhodopsin mutants. *Biochemistry* **45**, 5430–5439.
65. Altenbach, C., Yang, K., Farrens, D. L., Farahbakhsh, Z. T., Khorana, H. G., and Hubbell, W. L. (1996) Structural Features and Light-Dependent Changes in the Cytoplasmic Interhelical E-F Loop Region of Rhodopsin: A Site-Directed Spin-Labeling Study. *Biochemistry* **35**, 12470–12478.
66. Anderson, L. L., Marshall, G. R., and Baranski, T. J. (2005) Expressed protein ligation to study protein interactions: Semi-synthesis of the G-protein α subunit. *Protein Pept. Lett.* **12**, 783–787.
67. Anderson, L. L., Marshall, G. R., Crocker, E., Smith, S. O., and Baranski, T. J. (2005) Motion of carboxyl terminus of G α is restricted upon G protein activation. A solution NMR study using semisynthetic G α subunits. *J. Biol. Chem.* **280**, 31019–31026.